A highly thermotolerant, trimeric SARS-CoV-2 receptor binding domain derivative elicits high titers of neutralizing antibodies

Sameer Kumar Malladi[a], Unnatiben Rajeshbhai Patel[b], Randhir Singh[b], Suman Pandey[b], Sahil Kumar[c], Savitha Gayathri[a], Parismita Kalita[a], Ishika Pramanick[a], Poorvi Reddy[b], Nidhi Girish[b], Aditya Upadhyaya[b], Mohammad Suhail Khan[a], Madhuraj Bhat[b], Shailendra Mani[d], Sankar Bhattacharyya[d], Samreen Siddiqui[e], Akansha Tyagi[e], Sujeet Jha[e], Rajesh Pandey[f], Somnath Dutta[a], Rajesh P. Ringe[c], Raghavan Varadarajan*[, a, g]

[a] Molecular Biophysics Unit (MBU), Indian Institute of Science, Bengaluru, India

[b] Mynvax Private Limited, ES12, Entrepreneurship centre, SID, Indian Institute of Science, Bengaluru, India

[c] Virology Unit, Institute of Microbial Technology, Council of Scientific and Industrial Research (CSIR), Sector 39-A, Chandigarh 160036, India

[d] Translational Health Science and Technology Institute, NCR Biotech Science Cluster, 3rd Milestone, Gurugram-Faridabad Expressway, Faridabad-121001

[e] Max Super Speciality Hospital (A Unit of Devki Devi Foundation), Max Healthcare, Delhi-1100017, India

[f] INtegrative GENomics of HOst-PathogEn (INGEN-HOPE) laboratory, CSIR-Institute of Genomics and Integrative Biology (CSIR-IGIB), Mall Road, Delhi-110007, India

[g] Jawaharlal Nehru Centre for Advanced Scientific Research, Jakkur, Bengaluru, India

* Corresponding author: Raghavan Varadarajan
Email: varadar@iisc.ac.in, PHONE: +91-80-22932612, FAX: +91-80-23600535

Running title: Thermotolerant trimeric RBD immunogen

Keywords: glycosylation, thermostable, ACE2

Abstract

The Receptor Binding Domain of SARS-CoV-2 is the primary target of neutralizing antibodies. We fused our previously described, highly thermotolerant glycan engineered monomeric RBD to a heterologous non-immunogenic trimerization domain derived from cartilage matrix protein. The protein was expressed at a good yield of ~80-100 mg/liter in Expi293 cells, as well as in both CHO and HEK293 stable cell lines. The designed trimeric RBD was observed to form homogeneous disulfide-linked trimers. When lyophilized, the trimer possessed remarkable functional stability to transient thermal stress of upto 100 °C and was stable to long term storage of over 4 weeks at 37 °C. Two immunizations with an AddaVax adjuvanted formulation elicited antibodies with high endpoint neutralizing titers against replicative virus with geometric mean titers of ~1114 and 1940 in guinea pigs and mice respectively. In pseudoviral assays, corresponding titers were ~3600 and ~16050, while the corresponding value for human convalescent sera was 137. Similar results were obtained with an Alhydrogel, CpG combination adjuvant. The same immunogen was expressed in *Pichia pastoris,* but this formed high molecular weight aggregates and elicited much lower ACE2 competing antibodies than mammalian cell expressed protein. The excellent thermotolerance, high yield, and robust immunogenicity of such trimeric RBD immunogens suggest that they are a promising modality to combat COVID-19.

Importance

SARS-CoV-2 is the causative agent of the ongoing COVID-19 pandemic. The viral surface exposed Spike glycoprotein is the target of neutralizing antibodies of which a major fraction targets the receptor binding domain (RBD). Thus RBD derived immunogens are attractive vaccine candidates. Monomeric, mammalian cell expressed RBD protein elicits low to moderate titers of neutralizing antibodies. We designed a highly expressed, trimeric RBD derivative with a non-immunogenic trimerization domain. In guinea pigs and mice respectively, this derivative induces 20-300 fold higher neutralizing antibody titers relative to convalescent human sera, while remaining conformationally intact after incubation for over four weeks at 37 °C and for ninety minutes at 100 °C when lyophilized. Such trimeric RBD formulations should not require a cold chain. Additionally, the high titers of neutralizing antibodies should buffer against viral sequence variation. These are both highly desirable attributes for a COVID-19 vaccine, especially in resource limited settings.

Introduction

The Coronavirus infectious disease 2019 (COVID-19) pandemic is caused by SARS-CoV-2 (1, 2). SARS-CoV-2 has led to ~83.3 million infections and ~1.8 million deaths worldwide as on 4th January, 2020 (3). The viral spike glycoprotein is the most abundant protein exposed on the viral surface and the primary target of host elicited humoral immune responses (4, 5, 14, 15, 6–13). Thus, there are a large number of COVID-19 vaccine candidates in various stages of development, with three candidates already granted emergency use authorisation. However, all of these are required to be stored either refrigerated or frozen. There is thus an unmet need for efficacious vaccines that can be stored for extended periods at room temperature. In addition, there are recent reports of new strains of the virus with enhanced transmissibility (16, 17). This emphasizes the urgent need to develop vaccine formulations that elicit high titers of neutralizing antibodies to buffer against viral sequence variation (18–20). Spike glycoprotein, like various Class I viral surface glycoproteins assembles as a trimer with each protomer composed of the surface exposed S1 subunit and membrane anchored S2 subunit (21). The S1 subunit consists of four independently folding domains: N-terminal domain (NTD), Receptor binding domain (RBD) and two short domains (SD1 and SD2) connected by linker regions (4, 5, 22). The receptor binding domain (RBD) contains the receptor binding motif (residues 438-505) that facilitates interaction with the ACE2 receptor. Subsequent fusion or endocytosis is mediated by the fusion peptide that constitutes the N-terminal stretch of the S2 subunit (21). It is now well understood that the majority of neutralizing antibodies target the RBD (6, 7, 9, 10, 23–28). Thus, various groups are involved in designing RBD-based immunogens (29, 30, 39, 40, 31–38). We have previously designed a glycan engineered RBD derivative that was highly thermotolerant and induced moderate titers of neutralizing antibodies (35). Monomeric versions of immunogens elicit lower binding and neutralizing antibodies than multimeric version (29, 35, 38, 41). Potential strategies to improve neutralizing antibody titers include

fusion protein containing repetitive antigenic proteins, Fc fusion based dimerization, nanoparticle design and display strategies, and VLP based display platforms (36–43). While effective, several display strategies lead to significant antibody titers against the display scaffold or oligomerization motif, such antibodies might either show undesirable side effects in a small fraction of individuals or direct the response away from the intended target after repeated immunizations. In an alternative strategy, we fused our previously described thermotolerant RBD (35) to a trimerization motif, namely a disulphide linked coiled-coil trimerization domain derived from human cartilage matrix protein (hCMP) to the N-terminus of mRBD. This trimerization domain is expected to be much less immunogenic in small animals due to its homology with the corresponding ortholog, than other widely used trimerization domains of bacterial or synthetic origin such as foldon or IZ (44). hCMP-mRBD expressed as homogenous trimers, possessed comparable thermal stability profiles to the corresponding monomer (35) and remain functional after over 4 weeks upon lyophilization and storage at 37 °C. The RBD presented on the scaffold protein was highly immunogenic in mice and guinea pigs when formulated with AddaVax or alum derived adjuvants. Oligomerization increased neutralizing antibody titers by ~25-120 fold when compared with the titers in human convalescent sera, providing a proof of principle for the design strategy. Stable *CHO* and *HEK293* cell lines expressing hCMP-mRBD were constructed and the corresponding protein was as immunogenic as the protein expressed from transient transfection. The very high thermotolerance, enhanced immunogenicity and non-immunogenic trimerization domain suggest that this trimeric mRBD is an attractive vaccine candidate without requirement of a cold-chain to combat COVID-19, especially in resource limited settings.

Results

Design of trimeric RBDs of SARS-CoV-2

We previously designed a monomeric glycan engineered derivative of the receptor binding domain termed mRBD (residues 332-532 possessing an additional glycosylation site at N532) that induced neutralizing antibodies in guinea pig immunizations (35). It is known that oligomerization of the native antigens can induce higher titers of binding and neutralizing antibodies (38, 39, 42, 45–49). We therefore fused mRBD to the disulfide linked trimerization domain derived from human cartilage matrix protein (hCMP) (residues 298-340). We have previously used this domain to successfully trimerize derivatives of HIV-1 gp120. These earlier derivatives were used to successfully elicit high titers of broadly reactive antibodies in guinea pigs, and rabbits. In rhesus macaques when combined with an MVA prime, the formulation conferred protection against heterologous challenge, without apparent adverse effects (50–52). In the closed state structure model of Spike-2P protein (PDB 6VXX, residues 332-532), the three RBDs are in the down conformation. We therefore wished to explore if a trimeric RBD display fusion to the hCMP trimerization domain (residues 298-340), would improve neutralizing antibody titers relative to the corresponding monomer. We separated the coaxially aligned hCMP trimerization domain C-terminal residue 340. Cα plane from the RBD N-terminal Cα plane by ~22 Å to eliminate any steric clashes (Figure 1A). The linker length was determined between the hCMP C-terminus residue 340 and RBD N-terminus residue 332 to be 38.6 Å in the modeled structure (Figure 1A). An eleven amino acid linker derived from HIV-1 gp120 V1 loop (EGTMMRGELKN) with three additional residues (ASS) resulting in a fourteen amino acid linker L14 will comfortably span this distance. We have used this trimerization domain-linker combination in our previously described HIV-1 gp120 trimer design (53). Finally, the trimeric hCMP-mRBD design consisted of the N-terminal hCMP trimeric coiled coil domain (residues 298-340) fused to the I332 residue of mRBD by the above

linker, followed by the cleavable His tag sequence described previously(35). (Figure 1B). The hCMP trimerization domain leads to formation of covalently stabilized trimers crosslinked by interchain disulfides in the hCMP domain. This design is termed hCMP-mRBD and hCMP pRBD where the "m" and "p"signifies expression in mammalian or *Pichia pastoris* cells, respectively.

Homogeneous trimers of hCMP-mRBD, possess comparable thermal stability to mRBD and lyophilized protein is stable at 37°C for at least four weeks

The trimeric hCMP-mRBD was first expressed by transient transfection in Expi293F suspension cells, followed by single step metal affinity chromatography (Ni-NTA) and tag cleavage. The purified protein was observed to be pure and trimeric by reducing and non-reducing SDS-PAGE (Figure 2A, 2B). The protein exists as a homogenous trimer in solution and molar mass was determined by SEC-MALS as 110 ±10 kDa, consistent with the presence of nine glycosylation sites in the trimer (Figure 2A, 2C). Negative stain EM analysis confirmed the trilobed arrangement of RBD structure (Figure 3, Supplementary Figure 1).

Trimeric hCMP-mRBD was observed to have comparable thermal stability (T_m: 47.6 °C) as monomeric mRBD (T_m: 50.3 °C) (Figure 2D) and bound both its cognate receptor ACE2 and a SARS-CoV-1 neutralizing antibody CR3022 with very high affinity (K_D <1nM) (Figure 2E) (35). hCMP-mRBD protein in solution was observed to retain functionality after 1hour exposure to temperatures as high as 70 °C (Figure 4A). The lyophilized trimeric mRBD was also observed to retain functionality to transient ninety minute thermal stress upto 99 °C (Figure 4B). Further, the protein remained natively folded and retained functionality in solution upto three days, and upto four weeks in the lyophilized state upon incubation at 37 °C (Figure 5A, 5B, 5C, 5D). Thermal tolerance to transient and extended thermal stress is a desirable

characteristic for deployment of vaccines in low resource settings in the absence of a cold-chain.

AddaVax™ adjuvated trimeric mRBD elicits high titers of binding, receptor competing and neutralizing antibodies

We assessed the immunogenicity of the trimeric hCMP-mRBD adjuvanted with both the MF59 like adjuvant AddaVax™ as well as Alhydrogel in combination with CpG in both guinea pig and mice animal models. Animals were immunized intramuscularly at day 0, followed by a boost at day 21 and second boost at day 42 (35). Two weeks post first boost, sera were assayed for binding, ACE2 receptor competing, and neutralizing antibodies. In the AddaVax™ adjuvanted group, mice were observed to elicit ~10-fold higher binding antibodies to mRBD compared to guinea pigs (GMT titer mice: 235253, guinea pig: 25600, $p = 0.0476$) and hCMP-mRBD (GMT titer mice: 540470, guinea pig: 58813, $p = 0.0397$) (Figure 6A, 6C). hCMP-mRBD immunized guinea pigs elicited 14-fold higher titers of Spike-2P binding antibodies (GMT: 44572) compared to monomeric mRBD immunized guinea pigs (GMT: 3200) from our previous study (35). Higher (16-fold) Spike-2P binding antibodies were induced in mice (GMT: 713155) compared to guinea pigs (GMT 44572)($p = 0.0079$) with hCMP-mRBD (Figure 6B). Further, ACE2-hFc receptor competing titers (ID50) were assayed and mice sera contained ~3.5-fold higher titers compared to guinea pig sera (Mice sera GMT ID_{50}: 2016 vs Guinea pig sera GMT ID_{50}: 590, p = not significant (ns)) (Figure 6F). Overall, after two immunizations the formulation was less immunogenic in guinea pigs than mice and one of the guinea pigs showed a poor response, probably because one of the doses was improperly administered, since after a third immunization, all animals had increased and similar titers. We also assayed the binding titers directed towards the hCMP trimerization domain and gp120

derived linker by utilizing the previously described hCMP V1cyc JRFL gp120 containing the same trimerization domain (45) and JRFL gp120 as antigens respectively. Mice sera produced 33-fold higher hCMP domain binding titers (GMT: 33779) compared to guinea pig sera (GMT: 1009) (p = 0.0397) (Figure 6D). Importantly, both mice and guinea pigs did not elicit any binding antibodies to the L14 linker derived from gp120 (Figure 6E). The total binding titer in ELISA measured against whole protein (ie; hCMP-mRBD) elicited in mice and guinea pigs are 16-fold and 58-fold higher (p = 0.0159) respectively compared to the scaffold hCMP directed titers even after two immunizations (Figure 6D).

Trimeric mRBD adjuvanted with Alhydrogel in combination with CpG (TLR9 agonist) induced similar mRBD binding antibody titers in both mice and guinea pigs (GMT titer: 102400) and 28-fold higher Spike-2P binding titers in mice (mice GMT titer: 409600 vs guinea pig: 58813, p = 0.0079). hCMP-mRBD titers were 7-fold higher in mice (GMT titer in mice : 409600 vs guinea pig : 58813, p = 0.0079) with higher hCMP specific titers also being induced in mice (GMT titer in mice: 33779 vs guinea pig: 2111, p = 0.0079). ACE2 receptor competition was assayed and mice sera competed 11-fold higher compared to guinea pig sera (GMT titer in mice: 7914 vs guinea pig: 712, p = 0.0079) (Figure 6F). Pseudovirus neutralization titers in mice sera (GMT ID_{50}: 42149 (Alhydrogel+CpG), 16048 (AddaVax™)) were 2.4 - 4.5 fold higher compared to guinea pig sera (GMT ID_{50}: 17930 (Alhydrogel+CpG), 3582 (AddaVax™), p = ns) (Figure 6G). These titers were considerably in excess of titers observed in convalescent patient plasma ($p < 0.0001$) with the same pseudovirus neutralization assay (Figure 6G, Supplementary Figure 2C) which had a GMT of 137. Finally, replicative SARS-CoV-2 virus neutralization by CPE was assessed as described previously (35) and mice sera were observed to elicit 2-fold higher titers (NT_{100} GMT: 761 (Alhydrogel +CpG), 1940 (AddaVax™), p = ns) compared to guinea pig (NT_{100} GMT: 364 (Alhydrogel +CpG), 1114(AddaVax™), p = ns) (Figure 6H). Both pseudoviral and ACE2 competition titers

correlated well with each other and with ACE2 competition titers (Supplementary Figure 2A, 2B, 2C). We conclude that hCMP mediated trimerization of mRBD led to elicitation of robust binding and neutralizing antibodies considerably in excess of those seen in convalescent sera. Additionally, we performed a dose sparing study involving 5 µg hCMP-mRBD adjuvanted with AddaVax™. The binding titers were observed to be similar to the 20 µg dose (GMT hCMP-mRBD: 2.3 x 10^5, GMT of Spike-2P: 9.4 x 10^5, GMT of hCMP-mRBD: 7.1 x 10^5, p = ns) (Supplementary Figure 3).

All four groups of mice and guinea pigs adjuvanted with either AddaVax or Alhydrogel in combination with CpG were boosted again at week 6 and two weeks after the boost sera was assayed. The AddaVax adjuvanted hCMP-mRBD elicited similar mRBD and Spike-2P binding titers (GMT: 1241675) and high ACE2 competing titers (mice GMT:13683, guinea pig GMT: 9977, p = ns) (Supplementary Figure 4A, 4F). The mice and guinea pigs elicited 21 and 111 fold higher whole protein titers (mice GMT: 1638400, guinea pig GMT: 409600) relative to titers directed against the hCMP trimerization domain (mice GMT:77604, guinea pig GMT:3675, p = 0.0079) (Supplementary Figure 4C, 4D). The Alhydrogel combined with CpG adjuvant groups continued to show markedly higher binding and competition titers in mice compared to guinea pigs (p = 0.0079). The mRBD (mice GMT:1241675, guinea pig GMT: 77604, p = 0.0079) and Spike-2P (mice GMT:540470, guinea pig GMT: 19401, p = 0.0079) titers were 16 and 28-fold higher respectively in mice (Supplementary Figure 4A, 4B). In mice, the ACE2 competing titers exceeded guinea pig titers by ~4 folds (mice GMT: 7577, guinea pig GMT: 1975, p = 0.0079) in the Alhydrogel +CpG formulation guinea pigs and mice elicited 84 and 37 fold higher whole protein titers respectively (guinea pig GMT: 713155, mice GMT: 1638400) relative to those elicited against the hCMP trimerization domain (guinea pig GMT: 8445, mice GMT: 44572, p = 0.0079) (Supplementary Figure 4C, 4D). None of the animals showed measurable gp120 binding titers. Animals remained healthy after the immunizations.

Properties of hCMP-mRBD expressed from permanent cell lines to further clinical development of hMCP-mRBD

Stable Chinese hamster ovary (*CHO*) and HEK293 suspension cell lines expressing the protein were constructed. Purified protein yields were 80-100 mg/liter, similar to those expressed in *Expi293* cells, and SDS-PAGE revealed the presence of disulfide linked trimers (Supplementary Figure 5). *CHO* expressed protein adjuvanted with SWE adjuvant (identical to AddaVax, but from a different manufacturer) was immunized in mice following a prime:boost:boost regime. The sera post first and second boost were assayed. The mRBD binding titers were similar (Week 5 GMT: 235253, Week 8 GMT: 409600, p = ns) and Spike-2P binding titers were 12-fold higher at week 8 (GMT: 409600) compared to week 5 (GMT: 33779) (p = 0.0079) (Supplementary Figure 6A, 6B). The hCMP binding titers increased from 2111 to 19400 at week 5 to 8 respectively (p = 0.0159) (Supplementary Figure 6C). ACE2 competing titers also increased from 982 to 4658 from week 5 to 8 respectively (p = 0.0079) (Supplementary Figure 6E). *CHO* expressed protein also did not induce any detectable gp120 binding titers (Supplementary Figure 6D).

hCMP-pRBD protein was also expressed in the methylotrophic yeast *P. pastoris* at a purified yield of ~7mg/liter. As observed previously with monomeric RBD (35), the protein was more heterogeneous and formed high molecular weight aggregates than mammalian cell expressed proteins (Supplementary Figure 7A). In mice, formulations with the AddaVax equivalent adjuvant, SWE (54), elicited low mRBD, Spike reactive titers (Supplementary Figure 7B, 7C, 7D) and hence this formulation was not pursued further.

Discussion

There are currently multiple COVID-19 vaccines that have been given emergency use approval and others with encouraging Phase I data (55) are in advanced clinical trials. However there remains a need for cheap, efficacious, COVID-19 vaccines that do not require a cold chain. We previously designed a thermotolerant, monomeric, glycan engineered RBD (residues 332-532) that elicited neutralizing antibodies. In the present study we sought to improve the immunogenicity without negatively altering biophysical and antigenic characteristics of the designed immunogen. We therefore designed a trimeric mRBD by fusion with the hCMP trimerization domain at the N-terminus of mRBD. Relative to other trimerization domains such as foldon and GCN4 derivatives (40, 56), this forms a trimer that is stabilized by intermolecular disulfides and hence will not dissociate, even at high dilutions. A fusion of hCMP with HIV-1 gp120 has been extensively tested in guinea pigs, rabbits and non-human primates as an HIV-1 vaccine candidate and showed promising immunogenicity without any apparent adverse effects (45, 51, 52). This trimerization sequence has sequence identities with the corresponding ortholog of 81 and 91% in mice and guinea pigs, consistent with the much lower hCMP titers in guinea pigs. Thus, the hCMP titers in humans are expected to be negligible, given 100% sequence identity with the host protein. Like our previously described monomeric mRBD, hCMP-mRBD shows remarkable thermotolerance. Lyophilized hCMP-mRBD was stable to extended storage at 37 °C for over four weeks and to transient 90 minute thermal stress of upto 100 °C. Trimerization of mRBD led to elicitation of 14 fold higher Spike-2P binding antibodies (hCMP-mRBD GMT: 44572.2 vs mRBD GMT: 3200) and 2.6 fold higher neutralizing antibodies (hCMP-mRBD GMT: 1114 vs mRBD GMT: 415) compared to those elicited by mRBD immunizations in guinea pigs from our previous study (35). No detectable antibodies were elicited against the short gp120 derived stretch present in the linker of hCMP-mRBD in either mice or guinea pigs. Neutralization titers produced are considerably

in excess of those seen in patient derived convalescent sera by factors of ~110 and ~306 folds in mice adjuvanted with AddaVax and Alhydrogel+CpG respectively (Figure 6). In mice, the formulation induced higher binding and neutralizing antibodies compared to guinea pigs, presumably owing to various differences in the two host immune systems. Trimeric RBD bound ACE2-hFc receptor and the conformation specific antibody CR3022 (57) tightly, with undetectable dissociation (Figure 2E). RBD-GCN4 trimers were recently used in receptor binding studies (40). The neutralization titers elicited by the present trimeric RBD compare well with pseudoviral neutralization titers produced by a two dose immunization schedule of nanoparticle displayed RBD adjuvanted with AddaVax (IC_{50} GMT of 5 µg RBD-12GS-I53-50: 20000, corresponding IC_{50} GMT of human convalescent sera: 60, ~330 fold higher compared to HCS) and the Novavax Spike-2P adjuvanted with Matrix-M1 in mice (CPE_{100} GMT: 20000, CPE_{100} HCS GMT: 983, ~20 fold higher compared to HCS) (38, 55). Additionally, hCMP-mRBD elicited higher neutralizing titers than a 5 µg mRNA based RBD-foldon trimer vaccine construct BNT162b1 tested in mice (IC_{50} GMT: 753, HCS IC_{50} GMT: 94, ~8 fold higher compared to HCS) (56). The already high Ace2 competition titers elicited after two immunizations were significantly boosted after a third immunization (Figure 6, Supplementary Figure 4F, 6E, 7D). In contrast to recently described, highly immunogenic multi-component nanoparticle systems (37, 38), the present single component, trimeric RBD might be easier to purify and manufacture and in humans should elicit a higher proportion of RBD directed antibodies because of its host derived trimerization sequence. In summary, the present study describes the design of a disulfide linked trimeric immunogen that is stable to long term thermal stress and induces robust neutralizing antibodies against SARS-CoV-2. The availability of permanent cell lines for the immunogen, now make it possible to proceed with further clinical development of this thermotolerant and highly immunogenic COVID-19 vaccine candidate.

Materials and Methods

Trimeric RBD, ACE2-hFc and antibody expression constructs

The present trimeric mRBD construct consists of an N-terminal trimerization domain of human cartilage matrix protein (hCMP) (hCMP residues 298-340) (accession number AAA63904) linked by a 14-residue flexible linker (ASSEGTMMRGELKN) derived from the V1 loop of HIV-1 JR-FL gp120 linked to RBD residues 332-532 (accession number YP_009724390.1) with an engineered glycosylation site (NGS) at N532 fused to an HRV-3C precision protease cleavage site linked to a 10x Histidine tag by a GS linker. This construct is named hCMP-mRBD and was cloned into the mammalian expression vector pCMV1 under control of a CMV promoter and efficient protein secretion was enabled by the tPA secretion signal peptide sequence. The hCMP-mRBD construct reincorporated a glycosylation motif "NIT" at the N-terminal of the mRBD recapitulating the native glycosylation site at N331 in SARS-CoV-2 RBD. CR3022 antibody heavy and light chain genes were synthesised and subcloned into pcDNA3.4 vector by Genscript (USA).

Purification of recombinant proteins expressed in *Expi293F* cells

hCMP-mRBD protein was purified from transiently transfected Expi293F cells following manufacturer's guidelines (Gibco, Thermofisher) as described previously (35). Briefly, 24 hours prior to transfection, cells were passaged at a density of $2x10^6$ cells/mL into prewarmed Expi293F expression media. On the day of transfection, cells were freshly diluted at a density of $4x10^6$ cells/mL and transiently transfected with the desired plasmids. Plasmid DNA (1μg per 1mL of Expi293F cells) was complexed with ExpiFectamine293 and transiently transfected into Expi293F cells. Post 18-20 hr, Enhancer 1 and 2 addition was performed following the manufacturer's protocol. At three days following transfection, spent media was utilized for

purification of secreted protein by Ni Sepharose 6 Fast flow affinity chromatography resin (GE Healthcare). PBS (pH 7.4) equilibrated column was bound with two-fold diluted supernatant. Protein bound resin was washed with ten-column volumes of 1xPBS (pH7.4) supplemented with 25mM imidazole. Bound protein was eluted in a gradient of 200-500 mM imidazole supplemented PBS (pH 7.4). Eluted proteins were dialysed against PBS (pH 7.4) using a dialysis membrane of 3-5kDa (MWCO) (40mm flat width) (Spectrum Labs). Protein concentration was determined by absorbance (A_{280}) using NanoDrop™2000c with the theoretical molar extinction coefficient calculated using the ProtParam tool (ExPASy).

Expression and Purification of hCMP-pRBD

The construct sequence was codon-optimized for expression in *Pichia Pastoris* and cloned into the vector pPICZαA containing a MATalpha signal sequence for efficient secretion. The resulting clone was named pInCV21R. The pInCV21R plasmid was linearized with *Pme*I enzyme (NEB, R0560) prior to transformation.

10 µg of linearized plasmid was used for transformation into *Pichia pastoris* X-33 strain by electroporation as described in the user manual for Pichia expression by Thermo Fisher Scientific. The transformants were selected by plating on YPDS (YPD Sorbitol) plates with 100 µg/ml and 1mg/ml Zeocin (Thermo Fisher Scientific, R25005) and incubating the plates at 30 ^{o}C for upto 3 days.

25 colonies from the YPDS plate with 1 mg/ml Zeocin were picked and screened for expression by inducing with 1 % methanol every 24 hrs. Culture tubes (15 ml) with 1ml BMMY media (pH 6.0) each were used for inducing the cultures for upto 120 hrs at 30 ^{o}C and 250 rpm. The expression levels were checked using a dot blot analysis with Anti-his tag antibodies conjugated with HRP enzyme. The colony showing the highest expression level was then

chosen for large scale expression. The large scale culture was grown in 2l baffled shake flasks with 350 ml volume of culture. The expression levels were monitored every 24 hrs using Sandwich-ELISA.

The culture was harvested by centrifugation at 12000g, and the supernatant was filtered through a 0.45 micron filter. The supernatant was then incubated with Ni Sepharose 6 Fast flow resin (GE Healthcare) for 2 hrs. The beads were washed with 50 column volumes of 1X PBS pH 7.4 supplemented with 20 mM Imidazole. The His tagged protein was then eluted using 1X PBS pH 7.4 supplemented with 300 mM Imidazole. The eluted fractions were assessed for purity on a 12 % SDS-PAGE. The appropriate fractions were then pooled and dialyzed against 1X PBS to remove Imidazole.

Tag removal

HRV-3C precision protease digestion was performed to remove the C-terminal 10xHis tag (hCMP-mRBD: HRV-3C = 50:1). HRV-3C digestion was performed for 16 hrs at 4 °C in PBS (pH 7.4). Ni Sepharose 6 Fast flow resin (GE Healthcare) affinity exclusion chromatography was performed to obtain the tagless protein (containing the tag C-terminal sequence: LEVLFQ). The unbound tagless proteins concentration was determined by absorbance (A_{280}) using NanoDrop™2000c with the theoretical molar extinction coefficient calculated using the ProtParam tool (ExPASy).

Cell lines, media and growth conditions for polyclonal stable cell lines

Flp-In™-293 (Thermo Fisher Scientific, Cat# R75007, Lot# 2220695) as well as Flp-In™-CHO (Thermo Fisher Scientific, Cat# R75807, Lot # 2127131) adherent cells were used for making COVID-19 antigen hCMP-mRBD-HRV-Tg (a stop codon after 'Q' of HRV3C site

LEVLFQGP) polyclonal stable cell line. The cell line encoded hCMP-mRBD sequence is thus identical to that obtained after tag removal following HRV3C protease cleavage of protein produced by transient transfection. These engineered cells harbour a single Flp-In™ target site from vector 'pFRT/lacZeo' which confers Zeocin resistance. We first engineered COVID-19 antigen expressing recombinant cells using these adherent cells and then adapted them to suspension conditions for protein production.

Adherent cell culture

Both of the above adherent cells were cultured either in T25 or T75 EasYFlask, with a TC surface, filter cap (Thermofisher Scientific Cat# 156367 and 156499) in a moist 8 % CO_2 incubator at 37 °C.

The adherent Flp-In™-293 cells were grown in DMEM, high glucose media (Thermo Fisher Scientific Catalog #: 11965118) supplemented with 10 % Fetal Bovine Serum (FBS), qualified Brazil (Thermo Fisher Scientific Cat# 10270106), 100 U/ml Penicillin Streptomycin (Thermo Scientific Cat#15140122) and 100 µg/ml Zeocin™ Selection Reagent (Thermofisher Scientific Cat# R25001).

The adherent Flp-In™-CHO cells were grown in Ham's F-12 Nutrient Mix media (Thermo Fisher Scientific Catalog #: Cat # 11765054) supplemented with 10% FBS, 100 U/ml Penicillin-Streptomycin and 100 µg/ml Zeocin™ Selection Reagent.

Plasmid and vector

The Flp-In™ T-REx™ core kit containing pOG44 (Flp recombinase expressing plasmid) and pcDNA5/FRT/TO (donor plasmid for gene of interest) was purchased from Invitrogen USA (Cat # K650001).

The gene of interest 'hCMP-mRBD-HRV-Tg' was PCR amplified from hCMP-mRBD pCMV1 vector using *Hind*III site containing forward primer (5'—TATATAAGCTTCTGCAGTCACCGTCCTTAGATC—3') and *Xho*I site containing reverse primer (5'—TATATCTCGAGTCACTGGAACAGCACCTCCAGGGAGCC—3').

The amplified PCR product was digested with *Hind*III and *Xho*I and subcloned into pcDNA5/FRT/TO restricted with the above two enzymes. The clone was confirmed by sequencing.

Generation of adherent polyclonal Flp-In stable lines

T25 flasks (5 ml media) having either adherent Flp-In™-293 or Flp-In™-CHO cells (~80 % confluent) were co-transfected with pOG44 (10 µg) and hCMP-mRBD-HRV-Tg-pcDNA5/FRT/TO (5µg) plasmid DNA using 35 µg of Lipofectamine™ 2000 Transfection Reagent (Thermo Fisher Scientific, Cat # 11668030) in serum free media as per the manufacturers instruction for 4 hr. After 4 h, the media was replaced with serum containing media. The cells were incubated for 16 h and then trypsinized using 1 ml of 1X-Tryple express enzyme (Thermofisher Scientific, Cat# 12604021) and seeded to a T75 flask containing 25 ml of desired media and incubated for further 24 h for FLP recombination. After 24h the media was replaced with fresh media having Hygromycin 100 µg/ ml (Thermofisher Scientific Cat# 10687010) for Flp-In™-293 and 750 µg/ ml for Flp-In™-CHO cells. Hygromycin resistant foci were observed after 3 days of selection. Media containing the desired amount of Hygromycin was changed after every 5 days mentioned above. After 18 days in case of Flp-In™-293 and 14 days in case of Flp-In™-CHO, the recombinant hygromycin resistant cells reached to 100% confluency. The secretion of the protein of interest (hCMP-mRBD-HRV-Tg) was confirmed from cell free media using western blotting with polyclonal Guinea pig sera against the same antigen. The confirmed polyclonal cells were frozen in liquid N_2 for long term

storage. The T75-flask grown polyclonal cells were adapted for shake flask suspension culture and used for protein production.

Shake flask suspension cell culture and protein production

The suspension cells were grown in 125 or 250-ml Nalgene™ single-use PETG Erlenmeyer flasks with plain bottom and vented closure (Thermofisher Scientific Cat# 4115-0125 or 4115-0250) at 125 rpm with moist 8% CO_2 incubator at 37°C or as specifically mentioned.

The stable adherent recombinant Flp-In™-293 cells were first trypsinized from the T75 flask and then grown in a suspension flask after adapting them to FreeStyle™ 293 Expression Medium (Thermofisher Scientific Cat# 12338018) supplemented with 2% FBS and 50 µg/ml Hygromycin B for ~6 generations (two passages, doubling time=24h). These ~300 million cells were then seeded to 100 ml serum free FreeStyle™ 293 Expression medium for protein production for 3 days. After 3 days the media was used for protein purification. The ~300 million cells were grown further in 100 ml media for 6 days under identical conditions and used again for protein purification with >95% cell viability.

The stable adherent recombinant Flp-In™-CHO cells were first trypsinized from a T75 flask and then grown in a suspension flask for direct adaptation to PowerCHO™ 2 Serum-free Chemically Defined Medium (Lonza, Cat# 12-771Q) supplemented with 8 mM L-Glutamine (Thermo Fisher Scientific, Cat# 25-030-081) with 50 µg/ml Hygromycin B. First cells were grown for ~8 generations (two passages, doubling time=24h) at 37 °C till ~3 million per ml density. ~300 million cells were then seeded in 100 ml medium for protein production for 3 days at 32°C. After 3 days the media was harvested for protein purification. The ~300 million cells were grown further in 100 ml media for 6 days under identical condition and media used for protein purification with >95% cell viability.

Tagless protein purification

The spent media from stable hCMP-mRBD-HRV-Tg-Flp-In™-293 or Flp-In™-CHO grown cells contained the expressed protein. Protein was purified using anion exchange chromatography. 100 ml cell free media was first dialyzed against 30mM Tris-HCl buffer pH 8.4 overnight at 4 °C using cellulose membrane dialysis tubing (10kDa molecular weight cutoff, Sigma, Cat # D9527-100FT). 2mL Q Sepharose^{Tm} Fast Flow beads (GE Healthcare, Cat# 17-0510-01) were equilibrated with 30mM Tris-HCl pH 8.4 and incubated for 1h at 4°C with the dialyzed sample. Protein elution was performed with a step gradient of 30mM Tris-Hcl pH 8.4. containing 20-500mM NaCl. The fractions were analyzed on a 10% SDS-PAGE gel and the pure fractions were pooled and further dialyzed against 1X-PBS buffer pH 7.4, overnight. The pure protein was analyzed on 10% oxidizing as well as reducing SDS PAGE for homogeneity and purity. Size exclusion chromatography utilizing Superose 6 10/300 Increase GL column with 1X PBS as running buffer at a flow rate of 0.5mL/ min on an ÄktaPure (GE) was performed to determine protein aggregation state.

SDS-PAGE analysis, Size exclusion chromatography (SEC) and SEC-MALS Protein purity was estimated by denaturing PAGE. Samples were denatured in SDS containing sample buffer by boiling in reducing (with β-mercaptoethanol) or non-reducing (without β-mercaptoethanol) conditions.

SEC profiles were obtained in 1xPBS buffer equilibrated analytical gel filtration Superdex-200 10/300GL column (GE healthcare) on an Äkta pure chromatography system. The peak area under the curve (AUC) was determined in the Evaluation platform using the peak integrate tool. For SEC-MALS (multi angle light scattering), a PBS (pH 7.4) buffer equilibrated analytical Superdex-200 10/300GL gel filtration column (GE healthcare) on a SHIMADZU HPLC was utilized to resolve hCMP-mRBD purified protein. Gel filtration resolved protein

peaks were subjected to in-line refractive index (WATERS corp.) and MALS (mini DAWN TREOS, Wyatt Technology corp.) detection for molar mass determination. The acquired data from UV, MALS and RI were analysed using ASTRA™ software (Wyatt Technology).

nanoDSF thermal melt studies

Equilibrium thermal unfolding of hCMP-mRBD (- 10xHis tag) protein, before or after thermal stress was carried out using a nanoDSF (Prometheus NT.48) as described previously(35). Two independent measurements were carried out in duplicate with 2-4 μM of protein in the temperature range of 15-95 °C at 100% LED power and initial discovery scan counts (350nm) ranging between 5000 and 10000. In all cases, when lyophilized protein was used, it was reconstituted in water, prior to DSF.

Negative Staining sample preparation and visualization by Transmission Electron Microscope

For visualization by a Transmission Electron Microscope, the sample was prepared by a conventional negative staining method. Briefly, the carbon-coated copper grid was glow discharged for 20 seconds at 20mA using Quorum GlowQube. Around 3.5 μl of hCMP-mRBD sample (0.1mg/ml) was added to the freshly glow discharged carbon-coated copper grid for 1 minute. The extra sample was blotted out. Negative staining was performed using freshly prepared 1% Uranyl Acetate solution for 20 seconds and the grid was air-dried before TEM imaging. The negatively stained sample was visualized at room temperature using a Tecnai T12 electron microscope equipped with a Tungsten filament operated at 120 kV. Images were recorded using a side-mounted Olympus VELITA (2KX2K) CCD camera at a calibrated 3.54 Å/pixel.

514 **Reference-free 2D classification using single-particle analysis**

515 The evaluation of micrographs was done with EMAN 2.1 (58). Around 6600 particles were
516 picked manually and extracted using e2boxer.py in EMAN2.1 software. Reference free 2D
517 classification of different projections of particle were calculated using simple_prime2D of
518 SIMPLE 2.1 software (59).

519

520 **SPR-binding of hCMP-mRBD analyte to immobilized ACE2-hFc/CR3022**

521 hCMP-mRBD protein kinetic binding studies to ACE2-hFc and CR3022 antibody were
522 performed on a ProteOn XPR36 Protein Interaction Array V.3.1 (Bio-Rad). The GLM sensor
523 chip was activated with sulfo-NHS and EDC (Sigma) reaction. Protein G (Sigma) was
524 covalently coupled following activation. ~3500-4000 RU of Protein G (10 µg/mL) was coupled
525 in 10mM sodium acetate buffer pH 4.5 at a flow rate of 30 µl/min for 300 seconds in desired
526 channels. Finally, 1M ethanolamine was used to quench the excess sulfo-NHS esters.
527 Following quenching, ligand immobilization was carried out at a flow rate of 5 µg/mL for 100
528 seconds. ACE2-hFc or CR3022 were immobilized at ~800 RU on desired channels excluding
529 a single blank channel that acts as the reference channel. hCMP-mRBD analyte interaction with
530 ligands was monitored by passing over the chip at a flow rate of 30 µL/min for 200 seconds,
531 and the subsequent dissociation phase was monitored for 600 seconds. An empty lane without
532 ligand immobilization was utilized for measuring non-specific binding. Following each kinetic
533 assay, regeneration was carried out with 0.1 M Glycine-HCl (pH 2.7). The ligand
534 immobilization cycle was repeated prior to each kinetic assay. Various concentrations of the
535 hCMP-mRBD (- 10xHis tag) (100 nM, 50 nM, 25 nM, 12.5 nM, 6.25 nM) in 1x PBST were
536 used for binding studies. The kinetic parameters were obtained by fitting the data to a simple
537 1:1 Langmuir interaction model using Proteon Manager.

538

SPR-binding of thermal stress subjected hCMP-mRBD analyte to immobilized ACE2-hFc

Lyophilized protein or protein in 1X PBS (0.2 mg/mL) was subjected to transient thermal incubation at the desired temperature in a thermal cycler for ninety or sixty minutes, respectively. Post thermal incubation, binding response was assessed at 100nM analyte concentration by SPR as mentioned in the previous section.

Mice and Guinea Pig Immunizations

Immunizations of BALBc mice (n=5/group, female, 3-4 weeks old, ~16-18 g) and Hartley strain guinea pigs (n=5/group, female, 6-8 weeks old, ~300 g) were performed with freshly adjuvanted (AddaVax™ (vac-adx-10)) protein (1:1 v/v Antigen : AddaVax™ ratio per animal/dose, 20 µg protein in 50 µl PBS (pH 7.4) and 50 µl AddaVax™) (InvivoGen, USA). Animals were immunized via the intramuscular route with two doses constituting prime and boost on Day 0 and 21 respectively. Sera were isolated from bleeds drawn prior to prime (day -2), post prime (day 14) and post boost (day 35). All animal studies were approved by the Institutional Animal Ethics committee (IAEC) (RR/IAEC/61-2019, Invivo/GP/084). In the case of Pichia expressed protein, the AddaVax equivalent adjuvant SWE was used.

ELISA- serum binding antibody end point titers

Desired antigens were coated (4 µg/mL, 50 µL/well, 1xPBS) on 96 well plates for two hours and incubated on a MixMate thermomixer (Eppendorf, USA) at 25 °C under constant shaking (300 rpm). Antigen immobilization was assessed by coating ACE2-hFc protein. Coated wells were washed with PBST (200µl/well) four times, and blocked using blocking solution (100 µL, 3% skimmed milk in 1xPBST) and then incubated at 25 °C for one hour, 300 rpm. Post blocking, antisera were diluted four-folds serially, starting 1:100 and incubated at 25 °C for 1

hour, 300 rpm. Post sera binding, three washes were performed (200 µL of 1xPBST/well). Following this, anti-Guinea Pig IgG secondary antibody (ALP conjugated, Rabbit origin) (diluted 1:5000 in blocking buffer) (50 µL/well) was added and incubated at 25 °C for 1 hour, 300 rpm (Sigma-Aldrich). Post incubation, four washes were performed (200 µL of 1xPBST/well) and incubated with pNPP liquid substrate (50 µL/well) (pNPP, Sigma-Aldrich) at 37 °C for 30 minutes, 300 rpm. Finally, the chromogenic signal was measured at 405 nm. The highest serum dilution possessing signal above cutoff (0.2 O.D. at 405 nm) was considered as the endpoint titer for ELISA.

ACE2-hFc competition ELISA

ACE2-hFc competition was performed as described previously (35). ELISA was Monomeric mRBD antigen was coated on 96 well plates and incubated at 25 °C (4 µg/mL in 1x PBS, 50 µl/well), overnight under constant shaking (300 rpm) on a MixMate thermomixer (Eppendorf, USA). Negative control wells were coated with Ovalbumin (4 µg/mL in 1x PBS, 50 µL/well). Following four washes with 1xPBST, the coated wells were blocked with blocking solution (100 µL 3% skimmed milk in 1xPBST) and incubated at 25 °C for 1 hour, 300 rpm. Post blocking, sera competition wells were incubated with two-fold serial dilutions of anti-sera (60µL) starting at a dilution of 1:10 and control wells were incubated with blocking solution alone. Post one hour incubation at 25°C, 300 rpm, three washes were performed with 1xPBST (200 µL of 1xPBST/well). An additional blocking step was performed at 25°C, 300 rpm for 1 hour. Post blocking, ACE2-hFc was added in excess (60 µL at 20µg/mL) and incubated at 25 °C, for 1 hour, 300 rpm. Next, three washes were performed (200 µL of PBST/well) and anti-Human IgG secondary antibody (Sigma-Aldrich) (ALP conjugated, Rabbit origin, diluted 1:5000 in blocking buffer) was added (50 µL/well) and incubated at 25 °C for 1 hour, 300 rpm. Following secondary antibody binding, four washes were performed (200 µL of PBST/well).

pNPP liquid substrate (50 µL/well) was added and incubated for 30 minutes at 37 °C, 300 rpm. Finally, the chromogenic signal was measured at 405 nm. The percent competition was calculated using the following equation:

$$\%\ \text{competition} = [\text{A(Control)} - \text{A (Sera Dilution)}] * 100 / [\text{A (Control)}]\ .$$

Where**,** A(Control) is the Absorbance of binding signal of ACE2-Fc and mRBD in the absence of sera, A (Sera dilution) is the Absorbance of binding signal of ACE2-hFc and mRBD preincubated with antisera.

Convalescent patient sera samples

Convalescent patient sera were drawn (n = 40) and assayed for pseudoviral neutralization as described in the following pseudovirus neutralization section. The ethics approval of human clinical samples were approved by Institute Human Ethical Committee (Approval No: **CSIR-IGIB/IHEC/2020-21/01**)

CPE based viral Neutralization assay

Mice and Guinea pig pre-immune (negative control) sera and post boost sera were assayed for virus neutralization. Sera were heat inactivated prior to performing the assay by incubation at 56 °C for one hour. 100$TCID_{50}$ of replicative SARS-CoV-2 (Isolate: USA-WA1/2020) virus (50 µL) and serum were premixed and incubated for one hour at 37°C in a 5% CO_2 incubator. The virus-serum incubated premix samples were serially diluted and plated in duplicates in VeroE6 cell containing 96 well plate (10^4/well) and cultured for 48/96 hours. Post incubation, virus induced cytopathic effect (CPE) was assessed and the neutralization titre was deemed as the highest serum dilution at which no CPE was observed under the microscope.

Production of Pseudotyped SARS-CoV-2 and pseudovirus neutralization assay

Pseudo viral neutralization assays were performed with SARS-CoV-2 pseudo virus harbouring reporter NanoLuc luciferase gene. Briefly, HEK293T cells were transiently transfected with plasmid DNA pHIV-1 NL4.3Δenv-Luc and Spike-Δ19-D614G by using Profection mammalian transfection kit (Promega Inc) following the instructions in the kit manual. Post 48 hours, the pseudovirus containing culture supernatant was centrifuged for 10 mins at 600 xg followed by filtration via 0.22 μm filters, and stored at -80 $^{\circ}$C until further use. 293T-hACE-2 (BEI resources, NIH, Catalog No. NR-52511) or Vero/TMPRSS2 (JCRB cell bank, JCRB #1818) cells expressing the ACE2 or ACE and TMPRSS2 receptors respectively were cultured in DMEM (Gibco) supplemented with 5 % FBS (Fetal Bovine Serum), penicillin-streptomycin (100 U/mL). Patient derived convalescent sera (n = 40) were tested for neutralization in both 293T-ACE-2 and Vero/TMPRSS2 cells whereas animal sera were tested only in Vero/TMPRSS2 cells. Neutralization assays were done in two replicates by using heat-inactivated animal serum or human COVID-19 convalescent serum (HCS). The pseudovirus (PV) was incubated with serially diluted sera in a total volume of 100 μL for 1 hour at 37 $^{\circ}$C. The cells (Vero/TMPRSS2 or 293T-hACE2) were then trypsinised and $1x10^4$ cells/well were added to make up the final volume of 200uL/well. The plates were further incubated for 48 hours in humidified incubator at 37 $^{\circ}$C with 5% CO_2. After 48 hours of incubation, 140 μL supernatant was removed and 50 μL Bright-Glo luciferase substrate (Promega Inc.) was added. After 2-3 minute incubation, 80 μL lysate was transferred to white plates and luminescence was measured by using Cytation-5 multi-mode reader (BioTech Inc.) The luciferase activity measured as Relative luminescence units (RLU) from SARS-CoV-2 pseudovirus in the absence of sera was used as reference for normalizing the RLUs of wells containing sera. Pseudovirus neutralization titers (ID_{50}) were determined as the serum dilution at which infectivity was blocked by 50%.

Statistical Analysis

The *p* values for ELISA binding titers, neutralization titers, ACE2 receptor competition titers were analysed with a two-tailed Mann-Whitney test using the GraphPad Prism software. The correlation coefficients for ACE2-hFc receptor competition, pseudovirus, live virus and 293T-ACE2/VeroE6-TMPRSS2 cell line pseudovirus neutralizations were analysed by Spearman correlation using the GraphPad Prism software.

Data Availability Statement

All the data are in the manuscript.

Declaration of Competing Interest

A provisional patent application has been filed for the RBD formulations described in this manuscript. R.V, S.K.M, S.P, R.S are inventors. R.V is a co-founder of Mynvax and S.P, R.S, U.R.P, P.R., M.D., N.G, and A.U are employees of Mynvax Private Limited.

Acknowledgements

We thank Dr. Neil King for kindly providing the ACE2-hFc fusion protein, and Drs. Lynda Stuart, and Dr. Harry Kleanthous of the Bill and Melinda Gates foundation for helpful discussions. We thank Dr. Barney Graham for kindly providing the Spike-2P construct, and Dr. John Moore for providing SARS-CoV-2 full-length spike construct. This work was funded by a grant from the Bill and Melinda Gates Foundation to RV (INV-005948). The following reagent NR-52281, SARS-Related Coronavirus 2, Isolate USA-WA1/2020 was deposited by the Centers for Disease Control and Prevention and obtained through BEI Resources, NIAID, NIH: SARS-Related Coronavirus 2, Isolate USA-WA1/2020. We thank BEI Resources for

providing 293T-ACE2 cells submitted by Dr. Jesse Bloom. We also acknowledge funding for infrastructural support from the following programs of the Government of India: DST-FIST, UGC Center for Advanced Study, MHRD-FAST, the DBT-IISc Partnership Program, and of a JC Bose Fellowship from DST to RV. Mynvax acknowledges funding support from IISc CSR grant for COVID19 vaccine work. S.K.M acknowledges the support of the MHRD-IISc doctoral fellowship. S.D. acknowledges the support of DBT Cryo-EM facility (BT/INF/22/SP22844/2017SM). S.M. and S.B. acknowledge the intramural funding received from THSTI under Translational Research Program grant. R.P. acknowledges the support of CSIR_IGIB grant (MLP-2005) and Fondation Botnar (CLP-0031). R.P.R. acknowledges the support of SERB grant (IPA/2020/000168).

Author Contributions

R.V., S.K.M., conceptualized the work, designed the studies. S.P., R.V., R.S., planned the animal studies. R.S., performed the stable cell line work. R.S., U.R.P., P.R., A.U., performed ELISA and ACE2-hFc competition experiments. S.P., N.G., performed hCMP-mRBD protein expression and S.K.M. performed the characterization. S.G. performed hCMP-pRBD protein expression and characterization. M.S.K., performed SEC-MALS. P.K., cloned the hCMP-mRBD gene. M.B. performed the animal immunizations. I.P., S.D. provided the EM data and analysis. S.M., S.B., provided CPE neutralizing antibody assay data. R.P.R., S.K., performed pseudovirus neutralization assays. S.S, A.T., S.J., R.P. provided convalescent human serum samples. S.K.M wrote the manuscript with contributions from each author. S.K.M, R.V., led the studies and edited the paper along with all co-authors.

References

1. Chan JF-W, Yuan S, Kok K-H, To KK-W, Chu H, Yang J, Xing F, Liu J, Yip CC-Y, Poon RW-S, Tsoi H-W, Lo SK-F, Chan K-H, Poon VK-M, Chan W-M, Ip JD, Cai J-P, Cheng VC-C, Chen H, Hui CK-M, Yuen K-Y. 2020. A familial cluster of pneumonia associated with the 2019 novel coronavirus indicating person-to-person transmission: a study of a family cluster. Lancet (London, England) 395:514–523.

2. Zhu N, Zhang D, Wang W, Li X, Yang B, Song J, Zhao X, Huang B, Shi W, Lu R, Niu P, Zhan F, Ma X, Wang D, Xu W, Wu G, Gao GF, Tan W, China Novel Coronavirus Investigating and Research Team. 2020. A Novel Coronavirus from Patients with Pneumonia in China, 2019. N Engl J Med 382:727–733.

3. WHO. 2020. Coronavirus Disease (COVID-19) Dashboard. World Heal Organ.

4. Wrapp D, Wang N, Corbett KS, Goldsmith JA, Hsieh C-L, Abiona O, Graham BS, McLellan JS. 2020. Cryo-EM structure of the 2019-nCoV spike in the prefusion conformation. Science 367:1260–1263.

5. Walls AC, Park Y-J, Tortorici MA, Wall A, McGuire AT, Veesler D. 2020. Structure, Function, and Antigenicity of the SARS-CoV-2 Spike Glycoprotein. Cell 181:281-292.e6.

6. Barnes CO, Jette CA, Abernathy ME, Dam K-MA, Esswein SR, Gristick HB, Malyutin AG, Sharaf NG, Huey-Tubman KE, Lee YE, Robbiani DF, Nussenzweig MC, West AP, Bjorkman PJ. 2020. SARS-CoV-2 neutralizing antibody structures inform therapeutic strategies. Nature 588:682–687.

7. Barnes CO, West AP, Huey-Tubman KE, Hoffmann MAG, Sharaf NG, Hoffman PR, Koranda N, Gristick HB, Gaebler C, Muecksch F, Lorenzi JCC, Finkin S, Hägglöf T, Hurley A, Millard KG, Weisblum Y, Schmidt F, Hatziioannou T, Bieniasz PD, Caskey M, Robbiani DF, Nussenzweig MC, Bjorkman PJ. 2020. Structures of Human Antibodies Bound to SARS-CoV-2 Spike Reveal Common Epitopes and Recurrent Features of Antibodies. Cell 182:828-842.e16.

8. Chi X, Yan R, Zhang J, Zhang G, Zhang Y, Hao M, Zhang Z, Fan P, Dong Y, Yang Y, Chen Z, Guo Y, Zhang J, Li Y, Song X, Chen Y, Xia L, Fu L, Hou L, Xu J, Yu C, Li J, Zhou Q, Chen W. 2020. A neutralizing human antibody binds to the N-terminal domain of the Spike protein of SARS-CoV-2. Science 369:650–655.

9. Robbiani DF, Gaebler C, Muecksch F, Lorenzi JCC, Wang Z, Cho A, Agudelo M, Barnes CO, Gazumyan A, Finkin S, Hägglöf T, Oliveira TY, Viant C, Hurley A, Hoffmann H-H, Millard KG, Kost RG, Cipolla M, Gordon K, Bianchini F, Chen ST, Ramos V, Patel R, Dizon J, Shimeliovich I, Mendoza P, Hartweger H, Nogueira L, Pack M, Horowitz J, Schmidt F, Weisblum Y, Michailidis E, Ashbrook AW, Waltari E, Pak JE, Huey-Tubman KE, Koranda N, Hoffman PR, West AP, Rice CM, Hatziioannou T, Bjorkman PJ, Bieniasz PD, Caskey M, Nussenzweig MC. 2020. Convergent antibody responses to SARS-CoV-2 in convalescent individuals. Nature 584:437–442.

10. Wu Y, Wang F, Shen C, Peng W, Li D, Zhao C, Li Z, Li S, Bi Y, Yang Y, Gong Y, Xiao H, Fan Z, Tan S, Wu G, Tan W, Lu X, Fan C, Wang Q, Liu Y, Zhang C, Qi J, Gao GF, Gao F, Liu L. 2020. A noncompeting pair of human neutralizing antibodies block COVID-19 virus binding to its receptor ACE2. Science 368:1274–1278.

11. Cao Y, Su B, Guo X, Sun W, Deng Y, Bao L, Zhu Q, Zhang X, Zheng Y, Geng C, Chai X, He R, Li X, Lv Q, Zhu H, Deng W, Xu Y, Wang Y, Qiao L, Tan Y, Song L, Wang G, Du X, Gao N, Liu J, Xiao J, Su X, Du Z, Feng Y, Qin C, Qin C, Jin R, Xie XS. 2020. Potent Neutralizing Antibodies against SARS-CoV-2 Identified by High-Throughput Single-Cell Sequencing of Convalescent Patients' B Cells. Cell 182:73-84.e16.

12. Kreer C, Zehner M, Weber T, Ercanoglu MS, Gieselmann L, Rohde C, Halwe S, Korenkov M, Schommers P, Vanshylla K, Di Cristanziano V, Janicki H, Brinker R, Ashurov A, Krähling V, Kupke A, Cohen-Dvashi H, Koch M, Eckert JM, Lederer S, Pfeifer N, Wolf T, Vehreschild MJGT, Wendtner C, Diskin R, Gruell H, Becker S, Klein F. 2020. Longitudinal Isolation of Potent Near-Germline SARS-CoV-2-Neutralizing Antibodies from COVID-19 Patients. Cell 182:843-854.e12.

13. Liu L, Wang P, Nair MS, Yu J, Rapp M, Wang Q, Luo Y, Chan JFW, Sahi V, Figueroa A, Guo X V., Cerutti G, Bimela J, Gorman J, Zhou T, Chen Z, Yuen K-Y, Kwong PD, Sodroski JG, Yin MT, Sheng Z, Huang Y, Shapiro L, Ho DD. 2020. Potent neutralizing antibodies against multiple epitopes on SARS-CoV-2 spike. Nature 584:450–456.

14. Zost SJ, Gilchuk P, Case JB, Binshtein E, Chen RE, Nkolola JP, Schäfer A, Reidy JX, Trivette A, Nargi RS, Sutton RE, Suryadevara N, Martinez DR, Williamson LE, Chen EC, Jones T, Day S, Myers L, Hassan AO, Kafai NM, Winkler ES, Fox JM, Shrihari S, Mueller BK, Meiler J, Chandrashekar A, Mercado NB, Steinhardt JJ, Ren K, Loo Y-M, Kallewaard NL, McCune BT, Keeler SP, Holtzman MJ, Barouch DH, Gralinski LE, Baric RS, Thackray LB, Diamond MS, Carnahan RH, Crowe JE. 2020. Potently neutralizing and protective human antibodies against SARS-CoV-2. Nature 584:443–449.

15. Zost SJ, Gilchuk P, Chen RE, Case JB, Reidy JX, Trivette A, Nargi RS, Sutton RE, Suryadevara N, Chen EC, Binshtein E, Shrihari S, Ostrowski M, Chu HY, Didier JE, MacRenaris KW, Jones T, Day S, Myers L, Eun-Hyung Lee F, Nguyen DC, Sanz I, Martinez DR, Rothlauf PW, Bloyet L-M, Whelan SPJ, Baric RS, Thackray LB, Diamond MS, Carnahan RH, Crowe JE. 2020. Rapid isolation and profiling of a diverse panel of human monoclonal antibodies targeting the SARS-CoV-2 spike protein. Nat Med 26:1422–1427.

16. Kemp SA, Harvey WT, Datir RP, Collier DA, Ferreira I, Carabelli AM, Robertson DL, Gupta RK. 2020. Recurrent emergence and transmission of a SARS-CoV-2 Spike deletion ΔH69/V70. bioRxiv 2020.12.14.422555.

17. Korber B, Fischer WM, Gnanakaran S, Yoon H, Theiler J, Abfalterer W, Hengartner N, Giorgi EE, Bhattacharya T, Foley B, Hastie KM, Parker MD, Partridge DG, Evans CM, Freeman TM, de Silva TI, McDanal C, Perez LG, Tang H, Moon-Walker A, Whelan SP, LaBranche CC, Saphire EO, Montefiori DC, Angyal A, Brown RL, Carrilero L, Green LR, Groves DC, Johnson KJ, Keeley AJ, Lindsey BB, Parsons PJ, Raza M, Rowland-Jones S, Smith N, Tucker RM, Wang D, Wyles MD. 2020. Tracking Changes in SARS-CoV-2 Spike: Evidence that D614G Increases Infectivity of the COVID-19 Virus. Cell 182:812-827.e19.

18. Andreano E, Piccini G, Licastro D, Casalino L, Johnson N V, Paciello I, Monego SD, Pantano E, Manganaro N, Manenti A, Manna R, Casa E, Hyseni I, Benincasa L, Montomoli E, Amaro RE, McLellan JS, Rappuoli R. 2020. SARS-CoV-2 escape in vitro from a highly neutralizing COVID-19 convalescent plasma. bioRxiv 2020.12.28.424451.

19. Greaney AJ, Loes AN, Crawford KHD, Starr TN, Malone KD, Chu HY, Bloom JD. 2021. Comprehensive mapping of mutations to the SARS-CoV-2 receptor-binding domain that affect recognition by polyclonal human serum antibodies. bioRxiv 2020.12.31.425021.

20. Kim Y-I, Kim S-M, Park S-J, Kim E-H, Yu K-M, Chang J-H, Kim EJ, Casel MAB, Rollon R, Jang S-G, Um J, Song M-S, Jeong HW, Kim E-G, Kim Y, Kim SY, Park J-S, Park MS, Kwon G-Y, Yeo SG, Lee S-A, Choi YJ, Jung JU, Choi YK. 2021. Critical role of neutralizing antibody for SARS-CoV-2 reinfection and transmission. Emerg Microbes Infect 1–28.

21. Shang J, Wan Y, Luo C, Ye G, Geng Q, Auerbach A, Li F. 2020. Cell entry mechanisms of SARS-CoV-2. Proc Natl Acad Sci 117:11727–11734.

22. Bosch BJ, van der Zee R, de Haan CAM, Rottier PJM. 2003. The Coronavirus Spike Protein Is a Class I Virus Fusion Protein: Structural and Functional Characterization of the Fusion Core Complex. J Virol 77:8801–8811.

23. Brouwer PJM, Caniels TG, van der Straten K, Snitselaar JL, Aldon Y, Bangaru S, Torres JL, Okba NMA, Claireaux M, Kerster G, Bentlage AEH, van Haaren MM, Guerra D, Burger JA, Schermer EE, Verheul KD, van der Velde N, van der Kooi A, van Schooten J, van Breemen MJ, Bijl TPL, Sliepen K, Aartse A, Derking R, Bontjer I, Kootstra NA, Wiersinga WJ, Vidarsson G, Haagmans BL, Ward AB, de Bree GJ, Sanders RW, van Gils MJ. 2020. Potent neutralizing antibodies from COVID-19 patients define multiple targets of vulnerability. Science 369:643–650.

24. Huo J, Zhao Y, Ren J, Zhou D, Duyvesteyn HME, Ginn HM, Carrique L, Malinauskas T, Ruza RR, Shah PNM, Tan TK, Rijal P, Coombes N, Bewley KR, Tree JA, Radecke J, Paterson NG, Supasa P, Mongkolsapaya J, Screaton GR, Carroll M, Townsend A, Fry EE, Owens RJ, Stuart DI. 2020. Neutralization of SARS-CoV-2 by Destruction of the Prefusion Spike. Cell Host Microbe 28:445-454.e6.

25. Pinto D, Park Y-J, Beltramello M, Walls AC, Tortorici MA, Bianchi S, Jaconi S, Culap K, Zatta F, De Marco A, Peter A, Guarino B, Spreafico R, Cameroni E, Case JB, Chen RE, Havenar-Daughton C, Snell G, Telenti A, Virgin HW, Lanzavecchia A, Diamond MS, Fink K, Veesler D, Corti D. 2020. Cross-neutralization of SARS-CoV-2 by a human monoclonal SARS-CoV antibody. Nature 583:290–295.

26. Rogers TF, Zhao F, Huang D, Beutler N, Burns A, He W-T, Limbo O, Smith C, Song G, Woehl J, Yang L, Abbott RK, Callaghan S, Garcia E, Hurtado J, Parren M, Peng L, Ramirez S, Ricketts J, Ricciardi MJ, Rawlings SA, Wu NC, Yuan M, Smith DM, Nemazee D, Teijaro JR, Voss JE, Wilson IA, Andrabi R, Briney B, Landais E, Sok D, Jardine JG, Burton DR. 2020. Isolation of potent SARS-CoV-2 neutralizing antibodies and protection from disease in a small animal model. Science 369:956–963.

27. Shi R, Shan C, Duan X, Chen Z, Liu P, Song J, Song T, Bi X, Han C, Wu L, Gao G, Hu X, Zhang Y, Tong Z, Huang W, Liu WJ, Wu G, Zhang B, Wang L, Qi J, Feng H, Wang F-S, Wang Q, Gao GF, Yuan Z, Yan J. 2020. A human neutralizing antibody targets the receptor-binding site of SARS-CoV-2. Nature 584:120–124.

28. Wang Q, Zhang Y, Wu L, Niu S, Song C, Zhang Z, Lu G, Qiao C, Hu Y, Yuen K-Y, Wang Q, Zhou H, Yan J, Qi J. 2020. Structural and Functional Basis of SARS-CoV-2 Entry by Using Human ACE2. Cell 181:894-904.e9.

29. Chen W-H, Tao X, Peng B-H, Pollet J, Strych U, Bottazzi ME, Hotez PJ, Lustigman S, Du L, Jiang S, Tseng C-TK. 2020. Yeast-Expressed SARS-CoV Recombinant Receptor-Binding Domain (RBD219-N1) Formulated with Alum Induces Protective Immunity and Reduces Immune Enhancement. bioRxiv 2020.05.15.098079.

30. Mulligan MJ, Lyke KE, Kitchin N, Absalon J, Gurtman A, Lockhart S, Neuzil K, Raabe V, Bailey R, Swanson KA, Li P, Koury K, Kalina W, Cooper D, Fontes-Garfias C, Shi P-Y, Türeci Ö, Tompkins KR, Walsh EE, Frenck R, Falsey AR, Dormitzer PR, Gruber WC, Şahin U, Jansen KU. 2020. Phase I/II study of COVID-19 RNA vaccine BNT162b1 in adults. Nature 586:589–593.

31. Quinlan BD, Mou H, Zhang L, Guo Y, He W, Ojha A, Parcells MS, Luo G, Li W, Zhong G, Choe H, Farzan M. 2020. The SARS-CoV-2 receptor-binding domain elicits a potent neutralizing response without antibody-dependent enhancement. bioRxiv 2020.04.10.036418.

32. Ravichandran S, Coyle EM, Klenow L, Tang J, Grubbs G, Liu S, Wang T, Golding H, Khurana S. 2020. Antibody signature induced by SARS-CoV-2 spike protein immunogens in rabbits. Sci Transl Med 12:eabc3539.

33. Yang J, Wang W, Chen Z, Lu S, Yang F, Bi Z, Bao L, Mo F, Li X, Huang Y, Hong W, Yang Y, Zhao Y, Ye F, Lin S, Deng W, Chen H, Lei H, Zhang Z, Luo M, Gao H, Zheng Y, Gong Y, Jiang X, Xu Y, Lv Q, Li D, Wang M, Li F, Wang S, Wang G, Yu P, Qu Y, Yang L, Deng H, Tong A, Li J, Wang Z, Yang J, Shen G, Zhao Z, Li Y, Luo J, Liu H, Yu W, Yang M, Xu J, Wang J, Li H, Wang H, Kuang D, Lin P, Hu Z, Guo W, Cheng W, He Y, Song X, Chen C, Xue Z, Yao S, Chen L, Ma X, Chen S, Gou M, Huang W, Wang Y, Fan C, Tian Z, Shi M, Wang F-S, Dai L, Wu M, Li G, Wang G, Peng Y, Qian Z, Huang C, Lau JY-N, Yang Z, Wei Y, Cen X, Peng X, Qin C, Zhang K, Lu G, Wei X. 2020. A vaccine targeting the RBD of the S protein of SARS-CoV-2 induces protective immunity. Nature 586:572–577.

34. Zang J, Gu C, Zhou B, Zhang C, Yang Y, Xu S, Zhang X, Zhou Y, Bai L, Wu Y, Sun Z, Zhang R, Deng Q, Yuan Z, Tang H, Qu D, Lavillette D, Xie Y, Huang Z. 2020. Immunization with the receptor-binding domain of SARS-CoV-2 elicits antibodies cross-neutralizing SARS-CoV-2 and SARS-CoV without antibody-dependent enhancement. bioRxiv 2020.05.21.107565.

35. Malladi SK, Singh R, Pandey S, Gayathri S, Kanjo K, Ahmed S, Khan MS, Kalita P, Girish N, Upadhyaya A, Reddy P, Pramanick I, Bhasin M, Mani S, Bhattacharyya S, Joseph J, Thankamani K, Raj VS, Dutta S, Singh R, Nadig G, Varadarajan R. 2020. Design of a highly thermotolerant, immunogenic SARS-CoV-2 spike fragment. J Biol Chem jbc.RA120.016284.

36. Tai W, He L, Zhang X, Pu J, Voronin D, Jiang S, Zhou Y, Du L. 2020. Characterization of the receptor-binding domain (RBD) of 2019 novel coronavirus: implication for development of RBD protein as a viral attachment inhibitor and vaccine. Cell Mol Immunol 17:613–620.

37. Kit Tan T, Rijal P, Rahikainen R, Keeble AH, Hussain S, Harvey R, Hayes JW, Edwards JC, McLean RK, Martini V, Pedrera M, Thakur N, Dietrich I, Shelton H, Ludi A, Wilsden G, Zagrajek AK, Bialy D, Bhat S, Stevenson- P, Hollinghurst P, Tully M, Moffat K, Chiu C, Gray A, Azhar M, Mioulet V, Newman J, Burman A, Crossley S, Hammond JA, Tchilian E, Bailey D, Tuthill TJ, Graham SP, Huo J, Tree JA, Buttigieg

KR, Caroll MW, Daniels RS, McCauley JW, Howarth M, Townsend AR, Radcliffe Hospital J. 2020. A COVID-19 vaccine candidate using SpyCatcher multimerization of the SARS-CoV-2 spike protein receptor-binding domain induces potent neutralising antibody responses. bioRxiv 2020.08.31.275701.

38. Walls AC, Fiala B, Schäfer A, Wrenn S, Pham MN, Murphy M, Tse L V., Shehata L, O'Connor MA, Chen C, Navarro MJ, Miranda MC, Pettie D, Ravichandran R, Kraft JC, Ogohara C, Palser A, Chalk S, Lee E-C, Guerriero K, Kepl E, Chow CM, Sydeman C, Hodge EA, Brown B, Fuller JT, Dinnon KH, Gralinski LE, Leist SR, Gully KL, Lewis TB, Guttman M, Chu HY, Lee KK, Fuller DH, Baric RS, Kellam P, Carter L, Pepper M, Sheahan TP, Veesler D, King NP. 2020. Elicitation of Potent Neutralizing Antibody Responses by Designed Protein Nanoparticle Vaccines for SARS-CoV-2. Cell 183:1367-1382.e17.

39. Brouwer PJM, Brinkkemper M, Maisonnasse P, Dereuddre-Bosquet N, Grobben M, Claireaux M, de Gast M, Marlin R, Chesnais V, Diry S, Allen JD, Watanabe Y, Giezen JM, Kerster G, Turner HL, van der Straten K, van der Linden CA, Aldon Y, Naninck T, Bontjer I, Burger JA, Poniman M, Mykytyn AZ, Okba NMA, Schermer EE, van Breemen MJ, Ravichandran R, Caniels TG, van Schooten J, Kahlaoui N, Contreras V, Lemaître J, Chapon C, Ho Tsong Fang R, Villaudy J, Sliepen K, van der Velden YU, Haagmans BL, de Bree GJ, Ginoux E, Ward AB, Crispin M, King NP, van der Werf S, van Gils MJ, Grand R Le, Sanders RW. 2020. Two-component spike nanoparticle vaccine protects macaques from SARS-CoV-2 infection. bioRxiv 2020.11.07.365726.

40. Bouwman KM, Tomris I, Turner HL, Van Der 4 Woude R, Bosman GP, Rockx B, Herfst S, Haagmans BL, Ward AB, Boons G-J, De Vries RP. 2020. Multimerization-and glycosylation-dependent receptor binding of SARS-1 CoV-2 spike proteins. bioRxiv 2020.09.04.282558.

41. Dai L, Zheng T, Xu K, Han Y, Xu L, Huang E, An Y, Cheng Y, Li S, Liu M, Yang M, Li Y, Cheng H, Yuan Y, Zhang W, Ke C, Wong G, Qi J, Qin C, Yan J, Gao GF. 2020. A Universal Design of Betacoronavirus Vaccines against COVID-19, MERS, and SARS. Cell 182:722-733.e11.

42. Lainšček D, Fink T, Forstnerič V, Hafner-Bratkovič I, Orehek S, Strmšek Ž, Manček-Keber M, Pečan P, Esih H, Malenšek Š, Aupič J, Dekleva P, Plaper T, Vidmar S, Kadunc L, Benčina M, Omersa N, Anderluh G, Pojer F, Lau K, Hacker D, Correia B, Peterhoff D, Wagner R, Jerala R. 2020. Immune response to vaccine candidates based on different types of nanoscaffolded RBD domain of the SARS-CoV-2 spike protein. bioRxiv 2020.08.28.244269.

43. Powell AE, Zhang K, Sanyal M, Tang S, Weidenbacher PA, Li S, Pham TD, Pak JE, Chiu W, Kim PS. 2020. A single immunization with spike-functionalized ferritin vaccines elicits neutralizing antibody responses against SARS-CoV-2 in mice. bioRxiv 2020.08.28.272518.

44. Sliepen K, van Montfort T, Melchers M, Isik G, Sanders RW. 2015. Immunosilencing a Highly Immunogenic Protein Trimerization Domain. J Biol Chem 290:7436–7442.

45. Kesavardhana S, Das R, Citron M, Datta R, Ecto L, Srilatha NS, DiStefano D, Swoyer R, Joyce JG, Dutta S, LaBranche CC, Montefiori DC, Flynn JA, Varadarajan R. 2017. Structure-based Design of Cyclically Permuted HIV-1 gp120 Trimers That Elicit Neutralizing Antibodies. J Biol Chem 292:278–291.

910 46. Marcandalli J, Fiala B, Ols S, Perotti M, de van der Schueren W, Snijder J, Hodge E,
911 Benhaim M, Ravichandran R, Carter L, Sheffler W, Brunner L, Lawrenz M, Dubois P,
912 Lanzavecchia A, Sallusto F, Lee KK, Veesler D, Correnti CE, Stewart LJ, Baker D, Loré
913 K, Perez L, King NP. 2019. Induction of Potent Neutralizing Antibody Responses by a
914 Designed Protein Nanoparticle Vaccine for Respiratory Syncytial Virus. Cell 176:1420-
915 1431.e17.

916 47. Brouwer PJM, Antanasijevic A, Berndsen Z, Yasmeen A, Fiala B, Bijl TPL, Bontjer I,
917 Bale JB, Sheffler W, Allen JD, Schorcht A, Burger JA, Camacho M, Ellis D, Cottrell
918 CA, Behrens A-J, Catalano M, del Moral-Sánchez I, Ketas TJ, LaBranche C, van Gils
919 MJ, Sliepen K, Stewart LJ, Crispin M, Montefiori DC, Baker D, Moore JP, Klasse PJ,
920 Ward AB, King NP, Sanders RW. 2019. Enhancing and shaping the immunogenicity of
921 native-like HIV-1 envelope trimers with a two-component protein nanoparticle. Nat
922 Commun 10:4272.

923 48. Ueda G, Antanasijevic A, Fallas JA, Sheffler W, Copps J, Ellis D, Hutchinson GB,
924 Moyer A, Yasmeen A, Tsybovsky Y, Park Y-J, Bick MJ, Sankaran B, Gillespie RA,
925 Brouwer PJ, Zwart PH, Veesler D, Kanekiyo M, Graham BS, Sanders RW, Moore JP,
926 Klasse PJ, Ward AB, King NP, Baker D. 2020. Tailored design of protein nanoparticle
927 scaffolds for multivalent presentation of viral glycoprotein antigens. Elife 9.

928 49. López-Sagaseta J, Malito E, Rappuoli R, Bottomley MJ. 2016. Self-assembling protein
929 nanoparticles in the design of vaccines. Comput Struct Biotechnol J 14:58–68.

930 50. Kesavardhana S, Varadarajan R. 2014. Stabilizing the Native Trimer of HIV-1 Env by
931 Destabilizing the Heterodimeric Interface of the gp41 Postfusion Six-Helix Bundle. J
932 Virol2014/06/13. 88:9590–9604.

933 51. Jones AT, Chamcha V, Kesavardhana S, Shen X, Beaumont D, Das R, Wyatt LS,
934 LaBranche CC, Stanfield-Oakley S, Ferrari G, Montefiori DC, Moss B, Tomaras GD,
935 Varadarajan R, Amara RR. 2017. A Trimeric HIV-1 Envelope gp120 Immunogen
936 Induces Potent and Broad Anti-V1V2 Loop Antibodies against HIV-1 in Rabbits and
937 Rhesus Macaques. J Virol 92:e01796-17.

938 52. Jones AT, Shen X, Walter KL, LaBranche CC, Wyatt LS, Tomaras GD, Montefiori DC,
939 Moss B, Barouch DH, Clements JD, Kozlowski PA, Varadarajan R, Amara RR. 2019.
940 HIV-1 vaccination by needle-free oral injection induces strong mucosal immunity and
941 protects against SHIV challenge. Nat Commun 10:798.

942 53. Saha P, Bhattacharyya S, Kesavardhana S, Miranda ER, Ali PSS, Sharma D,
943 Varadarajan R. 2012. Designed cyclic permutants of HIV-1 gp120: implications for
944 envelope trimer structure and immunogen design. Biochemistry 51:1836–47.

945 54. de Jonge J, van Dijken H, de Heij F, Spijkers S, Mouthaan J, de Jong R, Roholl P, Adami
946 EA, Akamatsu MA, Ho PL, Brunner L, Collin N, Friede M, Ferreira JA, Luytjes W.
947 2020. H7N9 influenza split vaccine with SWE oil-in-water adjuvant greatly enhances
948 cross-reactive humoral immunity and protection against severe pneumonia in ferrets. npj
949 Vaccines 5:38.

950 55. Keech C, Albert G, Cho I, Robertson A, Reed P, Neal S, Plested JS, Zhu M, Cloney-
951 Clark S, Zhou H, Smith G, Patel N, Frieman MB, Haupt RE, Logue J, McGrath M,
952 Weston S, Piedra PA, Desai C, Callahan K, Lewis M, Price-Abbott P, Formica N, Shinde
953 V, Fries L, Lickliter JD, Griffin P, Wilkinson B, Glenn GM. 2020. Phase 1–2 Trial of a
954 SARS-CoV-2 Recombinant Spike Protein Nanoparticle Vaccine. N Engl J Med

383:2320–2332.

56. Vogel AB, Kanevsky I, Che Y, Swanson KA, Muik A, Vormehr M, Kranz LM, Walzer KC, Hein S, Güler A, Loschko J, Maddur MS, Ota-Setlik A, Tompkins K, Cole J, Lui BG, Ziegenhals T, Plaschke A, Eisel D, Dany SC, Fesser S, Erbar S, Bates F, Schneider D, Jesionek B, Sänger B, Wallisch A-K, Feuchter Y, Junginger H, Krumm SA, Heinen AP, Adams-Quack P, Schlereth J, Schille S, Kröner C, de la Caridad Güimil Garcia R, Hiller T, Fischer L, Sellers RS, Choudhary S, Gonzalez O, Vascotto F, Gutman MR, Fontenot JA, Hall-Ursone S, Brasky K, Griffor MC, Han S, Su AAH, Lees JA, Nedoma NL, Mashalidis EH, Sahasrabudhe P V, Tan CY, Pavliakova D, Singh G, Fontes-Garfias C, Pride M, Scully IL, Ciolino T, Obregon J, Gazi M, Carrion R, Alfson KJ, Kalina W V, Kaushal D, Shi P-Y, Klamp T, Rosenbaum C, Kuhn AN, Türeci Ö, Dormitzer PR, Jansen KU, Sahin U. 2020. BNT162b vaccines are immunogenic and protect non-human primates against SARS-CoV-2. bioRxiv 2020.12.11.421008.

57. Yuan M, Wu NC, Zhu X, Lee C-CD, So RTY, Lv H, Mok CKP, Wilson IA. 2020. A highly conserved cryptic epitope in the receptor binding domains of SARS-CoV-2 and SARS-CoV. Science 368:630–633.

58. Bell JM, Chen M, Baldwin PR, Ludtke SJ. 2016. High resolution single particle refinement in EMAN2.1. Methods 100:25–34.

59. Reboul CF, Eager M, Elmlund D, Elmlund H. 2018. Single-particle cryo-EM-Improved ab initio 3D reconstruction with SIMPLE/PRIME. Protein Sci 27:51–61.

Figure Legends

Figure 1. Design of trimeric mRBD. A. The design utilized the RBD (residues 332-532) from the closed state of the Spike-2P (PDB 6VXX) aligned coaxially with the hCMP trimerization domain, coordinates taken from the homolog CCMP (PDB:1AQ5, Chain 1.1). The N termini of mRBD are labelled as I332 and the hCMP trimerization domain C-termini are labelled as V340. The N, C termini Cα's form vertices of equilateral triangles. The N -terminal plane of RBD (I332) is separated from the C-terminal plane (V340) of the hCMP trimerization domain by ~22.1 Å to avoid steric clashes. The I332 terminus and V340 terminus are ~39 Å apart in the modelled structure and are connected by a 14-residue long linker. **B.** The final trimeric RBD construct consists of N-terminal hCMP trimerization domain fused to I332 of RBD by a linker (L14) followed by an HRV3C precision protease cleavage site and a 10x Histidine tag at the C-terminus.

Figure 2. Design and characterization of trimeric mRBD. A. SEC elution profile of trimeric hCMP-mRBD. **B.** SDS-PAGE of purified mRBD and hCMP-mRBD in reducing and non-reducing conditions demonstrating formation of disulfide-linked trimers. **C.** SEC-MALS of Ni-NTA purified hCMP-mRBD (MW: 110 ±10 kDa). The red, black and blue profiles are of the molar mass fit, molar mass and refractive index (RI) respectively. **D.** nanoDSF equilibrium thermal unfolding of purified trimeric hCMP-mRBD. **E.** SPR binding sensorgrams of trimeric mRBD binding to ACE2-hFc, and CR3022. The binding studies were performed with hCMP-mRBD proteins with concentrations of 100nM, 50nM, 25nM, 12.5nM and 6.25nM depicted from top to bottom, respectively.

Figure 3. Negative staining TEM analysis of hCMP-mRBD: A. A representative negative staining image of hCMP-mRBD protein. **B.** Representative reference free 2D class averages of hCMP-mRBD. 2D class averages indicate that hCMP-mRBD protein is monodisperse and stable. The protein forms a stable trimer. The bottom panel shows the enlarged view of class 1 and 7, trimeric hCMP-mRBD protein.

Figure 4. Characterization of trimeric hCMP-mRBD following transient exposure to elevated temperature. A. hCMP-mRBD in PBS at a concentration of 0.2 mg/ml was subjected to transient thermal stress for one hour and binding studies performed at 100nM. **B.** Lyophilized hCMP-mRBD was subjected to transient thermal stress for 90 minutes followed by reconstitution in water. The binding to ACE2-hFc was performed at 100nM. ACE2-hFc immobilized was 800RU. hCMP-mRBD is highly resistant to transient thermal stress.

Figure 5. hCMP-mRBD functionality after extended incubation at 37 °C. SPR sensorgrams of ACE2-hFc binding to hCMP-mRBD subjected to thermal stress **A.** hCMP-mRBD (0.2 mg/ml) in solution subjected to 37 °C incubation as a function of time (3-72 hr) **B.** Lyophilized hCMP-mRBD subjected to extended thermal stress at 4 °C and 37 °C for 2 and 4 weeks. 100nM of hCMP-mRBD was used as analyte. **C), D)** Equilibrium thermal unfolding monitored by nanoDSF. **C.** hCMP-mRBD (0.2mg/ml) subjected to 37 °C incubation in 1xPBS for upto 72 hours. **D.** nanoDSF of lyophilized hCMP-mRBD incubated for upto 4 weeks at 4 °C and 37 °C. The lyophilized protein was reconstituted in MilliQ grade water prior to thermal melt and SPR binding studies.

Figure 6. ELISA, ACE2 receptor inhibition, pseudovirus neutralization and replicative virus neutralization of sera elicited by hCMP-mRBD after two immunizations. Guinea pigs (GP) (○) and Mice (M) (●) were immunized at week 0 and 3 with 20μg of hCMP-mRBD adjuvanted with AddaVax™ (white panel) or Alhydrogel + CpG (gray panel). At 14 days post boost, sera were assayed for **A-E** ELISA binding titer against **A.** mRBD **B.** Spike-2P **C.** hCMP-mRBD **D**. hCMP V1cyc JRFL gp120 **E.** JRFL gp120 **F.** ACE2-hFc receptor competition binding titer **G.** Pseudoviral neutralization titer including Human Convalescent serum (◊) (HCS) (ID_{50}) utilizing pNL4-3.Luc. SARS-CoV-2 D614G Δ19 **H.** Replicative SARS-CoV-2 USA-WA1/2020 virus neutralization titer (NT_{100}). The black horizontal lines in each scatter plot represent Geometric Mean Titer (GMT). The pairwise titer comparisons were performed utilizing two-tailed Mann-Whitney test (* indicates $p < 0.05$, ** indicates $p < 0.01$, *** indicates $p < 0.001$, **** indicates $p < 0.0001$).

Figure 1

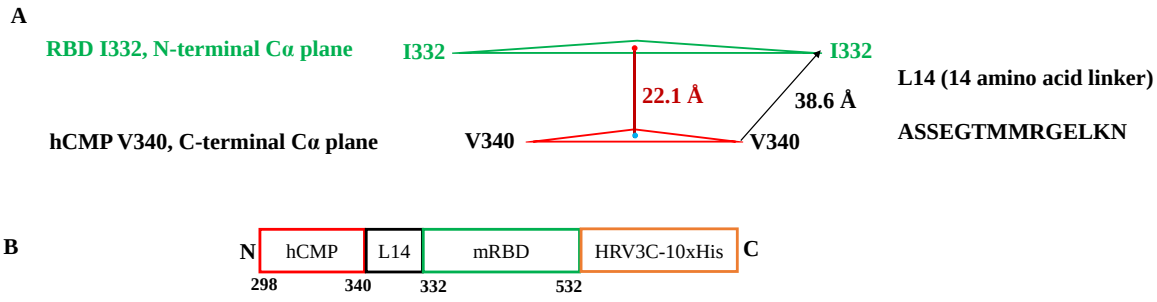

Figure 2

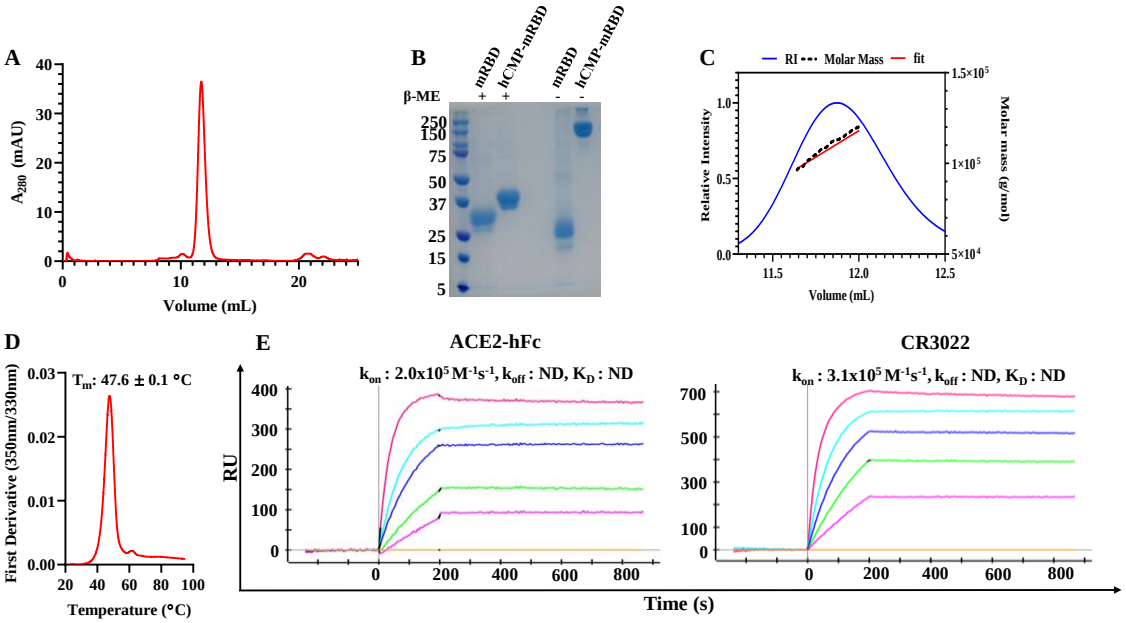

Figure 3

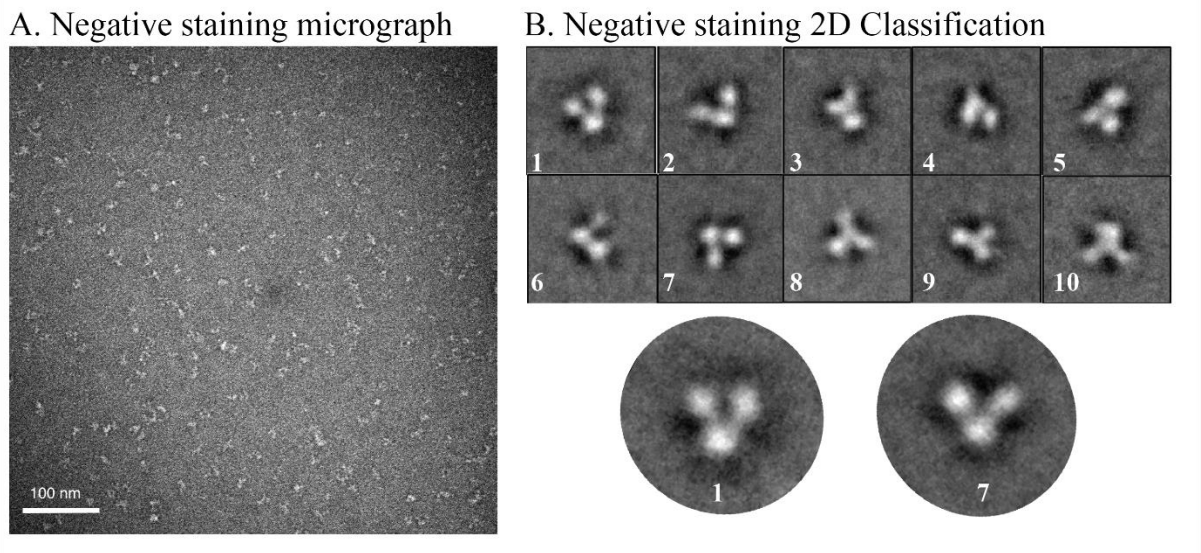

Figure 4

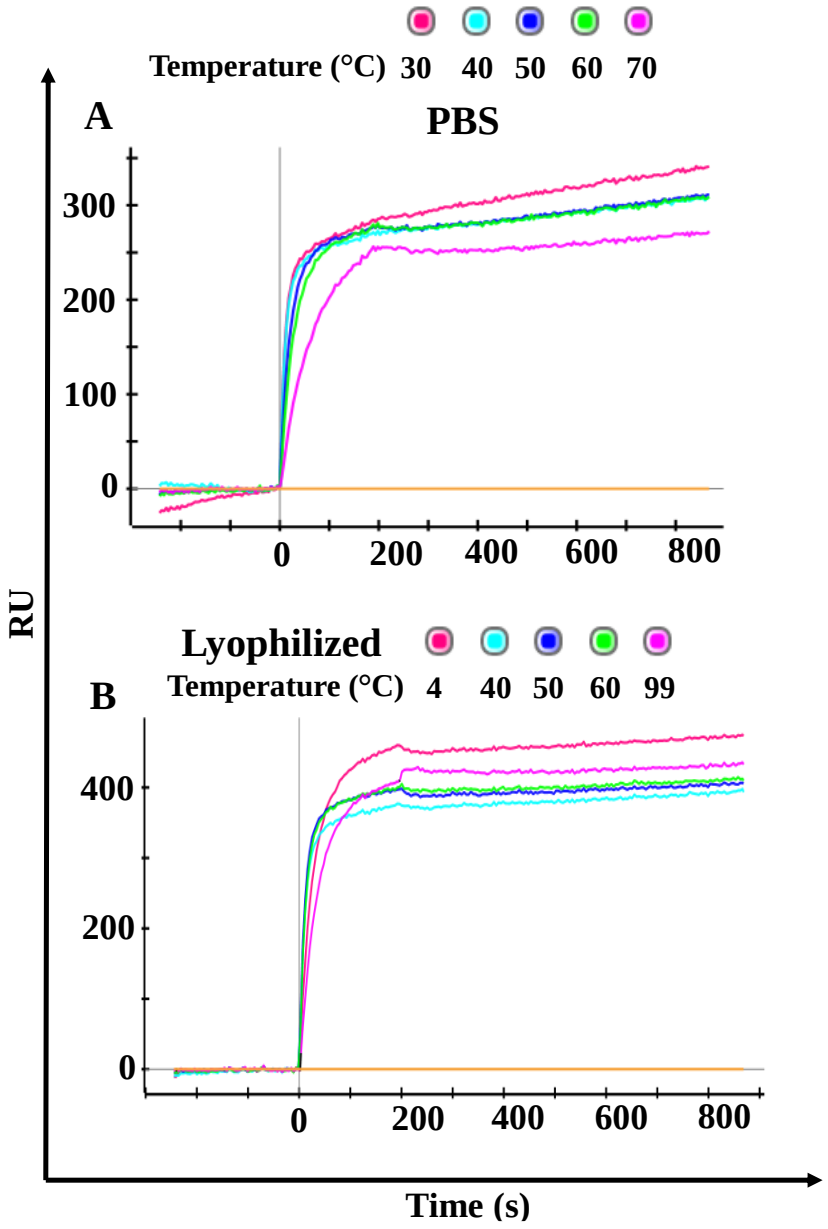

Figure 5

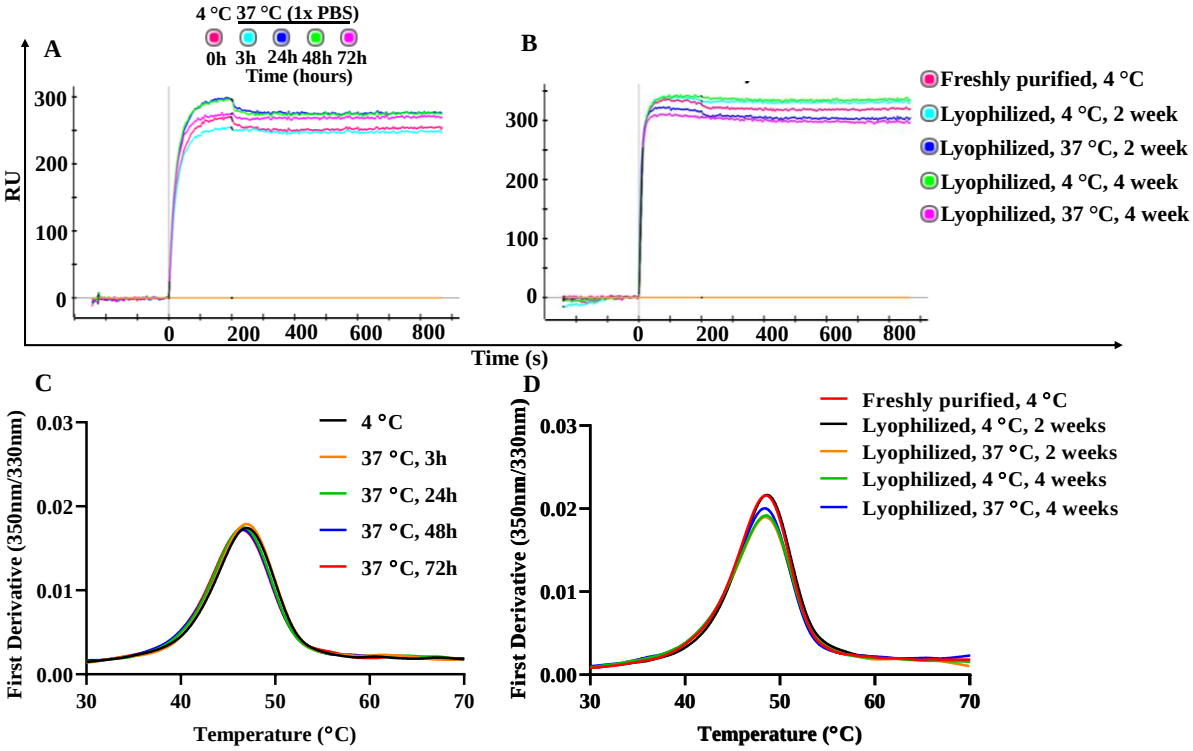

Figure 6